Water Capture Mechanisms at Zeolitic Imidazolate Framework Interfaces

Jackson C. Wagner[1], Kelly M. Hunter[1], Francesco Paesani[1,2]*, Wei Xiong[1,2,3]*

[1]Department of Chemistry and Biochemistry, University of California, San Diego, CA, USA, 92093

[2]Materials Science and Engineering Program, University of California, San Diego, CA, USA, 92093

[3]Department of Electrical and Computer Engineering, University of California, San Diego, CA, USA, 92093

ABSTRACT: Water capture mechanisms of zeolitic imidazolate framework ZIF-90 are revealed by differentiating the water clustering and the center pore filling step, using vibrational sum-frequency generation spectroscopy (VSFG) at a one-micron spatial resolution and state-of-the-art molecular dynamics (MD) simulations. Through spectral lineshape comparison between VSFG and IR spectra, the relative humidity dependence of VSFG intensity, and MD simulations, based on MB-pol, we found water clustering and center pore filling happen nearly simultaneously within each pore, with water filling the other pores sequentially. The integration of nonlinear optics with MD simulations provides critical mechanistic insights into the pore filling mechanism and suggests that the relative strength of the hydrogen bonds governs the water uptake mechanisms. This molecular-level detailed mechanism can inform the rational optimization of metal-organic frameworks for water harvesting.

Interest in atmospheric water capture materials has grown recently as the supply of fresh water becomes scarce. Metal-organic frameworks (MOFs), a class of porous crystalline solids composed of transition metal centers coordinated to organic linkers, hold great promise for water harvesting due to their high porosity and tunability. Understanding the water capture mechanisms is crucial to rationally designing MOFs for energy-efficient water capture.[1–4]

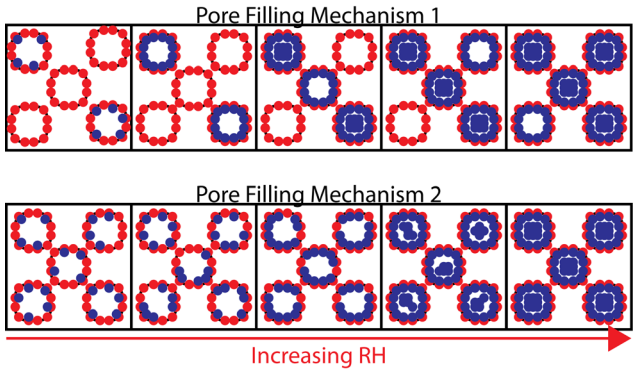

Figure 1 Proposed layer/cluster mechanism. In mechanism 1, individual pores are filled before additional pores are filled, while in mechanism 2, all pores fill simultaneously at a similar rate. Note: cluster and pore sizes are not to scale.

Among different water adsorption mechanisms in MOFs,[1–3] the layer/cluster adsorption is a common mechanism in which water clusters are first formed through nucleation on hydrophilic sites in the MOF (detailed description of water cluster in SI S6 Fig 13a). Then, water uptake at the center of the pore occurs through reversible pore filling.[2] While the mechanistic step is clear, molecular level details are missing.[5,6] For example, water clustering and center pore filling could occur sequentially on single pore levels, but simultaneously overall (Mechanism 1, Fig. 1). Alternatively, water clusters could form in every pore at a certain relative humidity (RH) and, after all pores have water clusters near the hydrophilic sites, center pore filling starts (Mechanism 2, Fig. 1).

The lack of mechanistic detail is largely due to the difficulty in separately probing water clustering and pore filling. The initial water cluster formation happens at the interior surface of MOFs, which requires interfacial specific techniques to probe. Adsorption/desorption isotherms,[7–9] a common method to study MOFs, only report the number of water molecules in the pores. Diffuse reflectance infrared Fourier transform spectroscopy (DRIFTS) can only probe the molecular details of bulk water in MOFs.[10–15] Although diffraction techniques have revealed molecular-level details of water adsorption in MOFs, applications to investigating the pore filling mechanism have been limited.[16–19] On the other hand, molecular dynamics (MD) simulations can provide molecular-level insights into interfacial processes, but often lack corresponding experimental comparison.[10,11,20–22]

Here, by selectively probing the water clustering step, using a spatially-resolved vibrational sum-frequency generation (VSFG) spectroscopy and MD simulations with the MB-pol[23–25] water model,[11] we study the water uptake mechanism of ZIF-90, a hydrophilic MOF that can adsorb water at low RH without open metal sites and be modified postsynthetically.[26,27] We find that ZIF-90 adsorbs water by mechanism 1. This study emphasizes the importance of interfacial-specific techniques,[28–33] determining that the competition between water-water and water-framework interactions dictates the uptake mechanism. Understanding ZIF-90 water uptake mechanism lays the foundation to further optimize its and other MOF's water harvesting function through post synthesis.

Two crucial technical aspects enable the micron-resolved VSFG to probe adsorbed water at interior MOF surfaces. First,

ZIF-90 lacks inversion symmetry ($I\bar{4}3m$ space group), making it VSFG active, which is evident by its strong second order non-resonant signal (broad feature at 2600 cm^{-1}).[34] Then, when water adsorbs on the interior interfaces, it becomes VSFG active, because the interactions between water and the hydrophilic groups of ZIF-90 template the water network, and transfer the symmetry from the framework to water. [35–41] This VSFG mechanism is different from the widely studied case of planar air/water interfaces.[42]

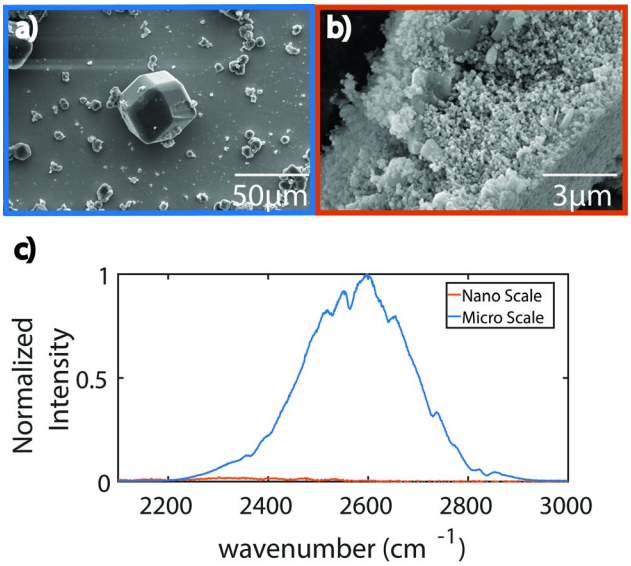

Figure 2. SEM images a) micron-sized and b) nanometer-sized ZIF-90 crystals. c) The SFG signal is large for the micron-sized crystal but neglegible for the nanocrystals.

Second, the VSFG microscope[43] (1.6 micron resolution) is necessary to probe single crystals, avoiding signals from randomly oriented crystals which, when ensemble averaged, cancel each other out.[44] The necessity of this effort is evident from the fact that only a single crystal of ZIF-90, having a diameter >10μm, (sample A, Fig. 2a and c), has a signal, while the aggregates of ZIF-90 nanocrystals (sample B, Fig. 2b and c, and SI Fig. 3) do not. In the following, we only focus on sample A and we also chose to study D_2O, instead of H_2O adsorption, to distinguish atmospheric H_2O adsorption by ZIF-90 during the sample transfer under dry conditions.[45–47]

As the RH is increased from 0% to 29% (Fig.3a starts from 23% for clarity, full range data see SI Fig.8), the overall non-resonant signal reduces. Similar signal reduction occurs when H_2O is adsorbed in this RH range (SI Fig. 6). Combining the fact that at this RH range no resonant molecular feature appears and the adsorption isotherms show very limited water uptake, we attribute the intensity reduction to an increase in refractive indices upon adsorption of a small amount of water,[48] which leads to a decrease in the Fresnel coefficients and ultimate reduction in the second-order response of the hydrated MOF (description in SI S2).[49] This small water adsorption prior to the major uptake is referred to as pre-adsorption.

As the RH increases, a dip near 2600 cm^{-1} becomes apparent at 31% RH (Fig. 3a). This feature appears exclusively during D_2O (in contrast to H_2O) adsorption. Combined with its center frequency, it is assigned to the OD stretch of adsorbed D_2O on the ZIF-90 interior surface, due to the symmetry transfer from ZIF-90.[35,37–39,50] Other possible origins of this spectral change[51] were ruled out (SI Fig. 5 and 6 for details).We extract the OD feature by treating the non-resonant signal as a local oscillator (see SI S4). Compared to bulk D_2O, OD features of both the bulk (DRIFTS) and interfacial (VSFG) D_2O in ZIF-90 exhibit

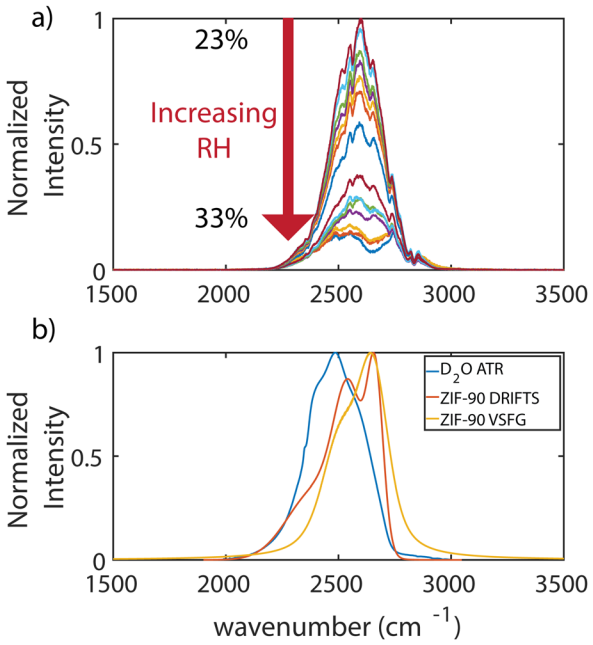

Figure 3. a) Raw VSFG spectra from 23% to 33% RH, b) an ATR spectrum of pure bulk D_2O, a DRIFTS spectrum at 43% RH and an extracted VSFG spectra at 33%RH of D_2O adsorbed by ZIF-90. No VSFG lineshape changes were observed above 33%.

blueshifts (Fig. 3b), suggesting weaker hydrogen-bond interactions experienced by the D_2O molecules in ZIF-90, which is supported by our previous MD simulations.[11]

Spectral fittings show that the DRIFTS spectra have three peaks at 2400 cm^{-1}, 2550 cm^{-1} and 2665 cm^{-1} (Fig. 4a), while VSFG spectra have two peaks centered at ~2515 cm^{-1} and 2630 cm^{-1} (Fig. 4b). Besides the Fermi resonance at 2400 cm^{-1}, the 2550 cm^{-1} and 2665 cm^{-1} peaks were assigned to the asymmetric and symmetric OD stretching modes.[11] The peak lineshape difference between VSFG and DRIFTS spectra suggest that the VSFG signal is not a phantom signal due to liquid water absorption.[51]

Despite a small redshift between the DRIFTS and VSFG spectra (~35 cm^{-1}), the overall peak positions are similar, which is somewhat counterintuitive. As explained above, VSFG probes D_2O bound to the aldehyde groups at the step of water clustering, whereas DRIFTS probes all D_2O inside the pore, at both water clustering and pore filling steps (see SI S6 and SI Fig. 13 for details). Based on MD simulation, if during the water cluster step D_2O is only bound to the aldehyde groups of ZIF-90, its OD frequency should be ~2720 cm^{-1}, significantly blueshifted compared to D_2O in the bulk region of the pore (~2600 and 2660 cm^{-1}, SI Fig 14). This blueshift is observed because the hydrogen bonding between D_2O and aldehyde groups is weaker than that between D_2O molecules.[11] Thus, the similar spectral positions in the DRIFTS and VSFG spectra suggest that instead of only binding to the organic linkers, D_2O molecules in the water clustering step experience a comparable local environment to the ones of pore filling steps.

A more unexpected result is that the RH dependence of the VSFG peak intensities closely follows the adsorption isotherm

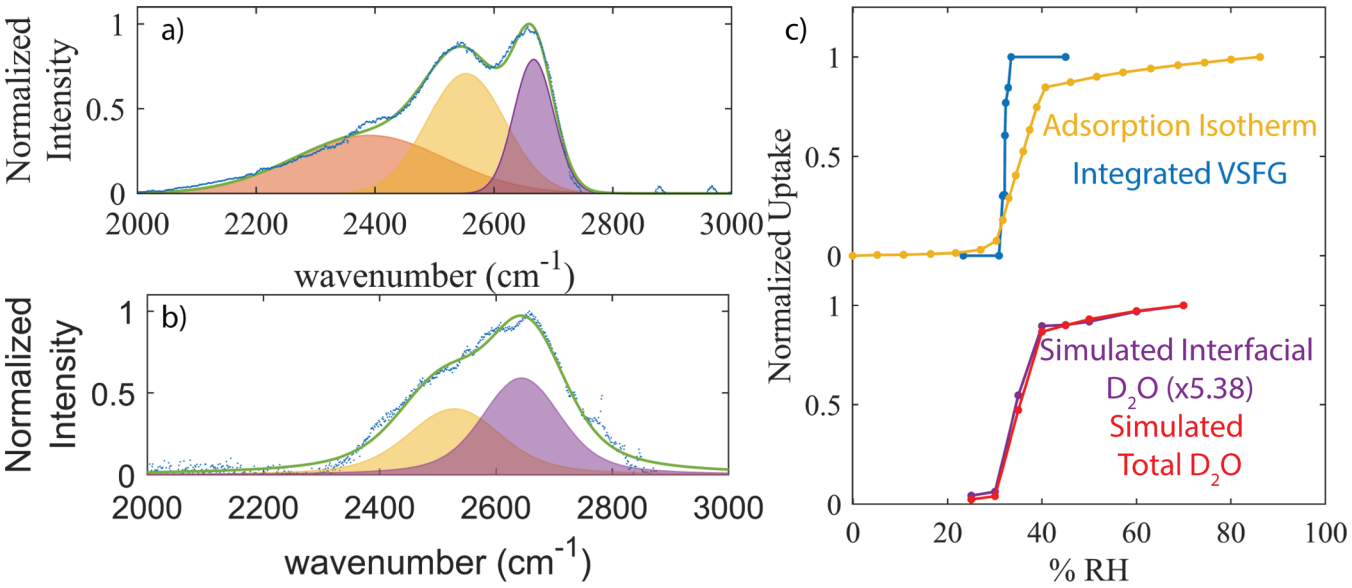

Figure 4. Fitting results for a) DRIFTS and b) VSFG at saturation. c) Experimental integrated VSFG intensity (blue), adsorption isotherm (yellow), bound D_2O that contribute to VSFG signal from simulation, N_{suf} (purple), and total simulated D_2O inside pore versus RH, N_{tot} (red). N_{suf} is calculated as the average number of water throughout the simulation that form a hydrogen bond to the carbonyl group of the framework (OW-o distance ≤ 3.5 Å and HW-OW-o angle ≤ 30°) for more than 400 fs, which is coherent lifetime of the OD oscillation.

(Fig. 4c). Since VSFG probes D_2O bound to the interior surfaces, the VSFG spectra are sensitive to the water clustering stages of D_2O uptake. In other words, the RH dependence of the VSFG signal suggests that the onset of water clustering and pore filling occur simultaneously. We note that the RH dependence of the DRIFTS intensity (SI Fig. 10) differs drastically from that of the VSFG spectrum because DRIFTS intensity scales nonlinearly with the adsorbate concentration.[12–15]

MD simulations with the MB-pol model provide molecular-level insights into the underlying molecular mechanism of D_2O uptake by ZIF-90. At 30% RH, the simulations indicate that instead of a uniform distribution across all pores, D_2O molecules localize into a single pore (Fig. 5a).[20] Only at 40% RH do D_2O molecules nearly uniformly occupy all pores (Fig. 5b). This result is robust against the initial distribution of D_2O molecules at every RH (SI S6 and SI Figs. 15-17).

We further plot the number of D_2O molecules adsorbed at interior surfaces (N_{suf}), which can contribute to the VSFG signal, as well as the total number of adsorbed D_2O molecules (N_{tot}) as a function of RH (Fig. 4c), to determine if water clustering and pore filling occur concurrently (mechanism 1) or sequentially (mechanism 2). Both N_{suf} and N_{tot} follow a similar trend and saturate at 40% when all pores are filled, agreeing with the RH dependence of the VSFG intensity and adsorption isotherm. This implies that water clustering and pore filling occur concurrently, with the D_2O molecules filling one pore after another, as in mechanism 1 (Fig. 1).

Our MD simulations further indicate that adsorption in a single pore is energetically favorable. When the D_2O molecules cluster in a single pore, the enthalpy of adsorption is ~2 kcal/mol lower than when the D_2O molecules are uniformly distributed (Fig. 5c and SI Fig.18). This result is explained by considering that water-carbonyl interactions are weaker than water-water interactions in ZIF-90. It should be noted that, due to slower orientational dynamics, the entropy of the D_2O molecules in ZIF-90 is larger than in the bulk and decreases as the RH increases (SI Tables S3-S6).[52–55] At the very early stages of uptake, the entropic term thus drives D_2O molecules to the interior surface of a pore where they offer additional hydrogen-bonding sites. Due to stronger water-water interactions (i.e., larger enthalpic term) additional D_2O molecules prefer to form hydrogen bonds with the surface-bound D_2O molecules, instead of binding to aldehyde groups in other pores.

Since water clustering and pore filling occur simultaneously, it follows that, although VSFG detects D_2O involved in the clustering step, these molecules, at the same time, experience hydrogen-bonding interactions with other D_2O molecules in the pore, which explains why the positions of the D_2O peaks in the DRIFTS and VSFG spectra are similar. This conclusion is supported by the vibrational densities of states calculated for bulk D_2O and D_2O adsorbed at the interior of the ZIF-90 pores (SI Fig. 14).

For ZIF-90, water clustering and pore filling occur in single pores before other pores are filled, driven by initial entropic gains followed by increasing enthalpic contributions due to stronger water-water interactions than water-framework interactions. This mechanism is similar to the nucleation of water dispersed in a hydrophobic medium[56] and was also reported for the hydrophobic ZIF-8.[20] However, it is unexpected for ZIF-90, which is hydrophilic. Thus, this work shows that when designing new MOFs for water harvesting, it is important to consider both entropic effects and the relative strength of the water-framework and water-water interactions, in addition to the hydrophilicity/hydrophobicity of the framework which is often considered as the main factor that determines water uptake. Molecular-level mechanisms of water uptake evolution in MOFs remain to be further explored to guide fine tuning of these materials for better performance.[19] The integration of advanced spectroscopic techniques and computer simulations described here provide such a capability to better understand and optimize guest molecules capturing mechanism for many host materials.

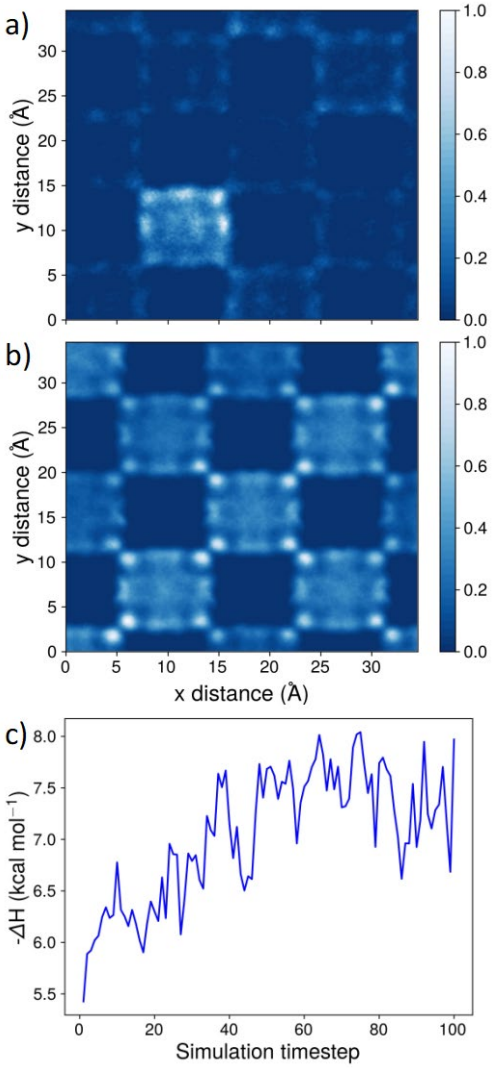

Figure 4. (a) At 30% RH, water preferentially clusters in single pores, and only the surface site on this specific unit cells are occupied, whereas (b) at 40% RH, water evenly distributes among pores with all surface sites occupied. (c) The enthalpy of adsorption at 30% RH of water in ZIF-90 shows that when water is initally evenly distributed in the materials, its enthalpy increases by clustering into single unit cells.

ASSOCIATED CONTENT

SUPPLEMENTARY INFORMATION

Experimental methods, control and characterization experiments, DRIFTS and VSFG fitting methods and results, and simulation methods and additional results. This material is available free of charge via the Internet at http://pubs.acs.org

AUTHOR INFORMATION

Corresponding Author

* Francesco Paesani, fpaesani@ucsd.edu
* Wei Xiong, w2xiong@ucsd.edu

Author Contributions

The manuscript was written through contributions of all authors. All authors have given approval to the final version of the manuscript.

Funding Sources

This work is supported by Department of Energy, Basic Energy Science (BES) Office, Condensed Phase and Interfacial Molecular Science (CPIMS) Program (Award No. DESC0019333). All simulations used resources of the National Energy Research Scientific Computing Center (NERSC), supported by Department of Energy BES Office under contract DE- AC02-05CH11231. The VSFG microscope is developed under the support of National Science Foundation, Division of Chemistry, Major Research Instrumentation program (MRI), CHE-1828666. SEM imaging was done in part at San Diego Nanotechnology Infrastructure (SDNI) of UCSD, an NSF designated National Nanotechnology Coordinated Infrastructure site, supported by NSF grant ECCS-1542148.

Notes

The authors declare no competing financial interests.

ACKNOWLEDGMENT

We acknowledge Dr. Mark Kalaj from Dr. Seth Cohen's group for synthesizing ZIF-90 MOF.

REFERENCES

(1) Hanikel, N.; Prévot, M. S.; Yaghi, O. M. MOF Water Harvesters. *Nat. Nanotechnol.* **2020**, *15* (5), 348–355. https://doi.org/10.1038/s41565-020-0673-x.

(2) Canivet, J.; Fateeva, A.; Guo, Y.; Coasne, B.; Farrusseng, D. Water Adsorption in MOFs: Fundamentals and Applications. *Chem. Soc. Rev.* **2014**, *43* (16), 5594–5617. https://doi.org/10.1039/c4cs00078a.

(3) Liu, X.; Wang, X.; Kapteijn, F. Water and Metal-Organic Frameworks: From Interaction toward Utilization. *Chem. Rev.* **2020**, *120* (16), 8303–8377. https://doi.org/10.1021/acs.chemrev.9b00746.

(4) Yu, M. H.; Liu, X. T.; Space, B.; Chang, Z.; Bu, X. H. Metal-Organic Materials with Triazine-Based Ligands: From Structures to Properties and Applications. *Coord. Chem. Rev.* **2021**, *427*, 213518. https://doi.org/10.1016/j.ccr.2020.213518.

(5) Bon, V.; Senkovska, I.; Evans, J. D.; Wöllner, M.; Hölzel, M.; Kaskel, S. Insights into the Water Adsorption Mechanism in the Chemically Stable Zirconium-Based MOF DUT-67-a Prospective Material for Adsorption-Driven Heat Transformations. *J. Mater. Chem. A* **2019**, *7* (20), 12681–12690. https://doi.org/10.1039/c9ta00825j.

(6) Nandi, S.; Aggarwal, H.; Wahiduzzaman, M.; Belmabkhout, Y.; Maurin, G.; Eddaoudi, M.; Devautour-Vinot, S. Revisiting the Water Sorption Isotherm of MOF Using Electrical Measurements. *Chem. Commun.* **2019**, *55* (88), 13251–13254. https://doi.org/10.1039/c9cc06012j.

(7) Li, Y.; Wang, X.; Xu, D.; Chung, J. D.; Kaviany, M.; Huang, B. H2O Adsorption/Desorption in MOF-74: Ab Initio Molecular Dynamics and Experiments. *J. Phys. Chem. C* **2015**, *119* (23), 13021–13031. https://doi.org/10.1021/acs.jpcc.5b02069.

(8) Solovyeva, M. V.; Shkatulov, A. I.; Gordeeva, L. G.; Fedorova, E. A.; Krieger, T. A.; Aristov, Y. I. Water Vapor Adsorption on CAU-10- X: Effect of Functional Groups on Adsorption Equilibrium and Mechanisms. *Langmuir* **2021**, *37* (2), 693–702. https://doi.org/10.1021/acs.langmuir.0c02729.

(9) Tan, B.; Luo, Y.; Liang, X.; Wang, S.; Gao, X.; Zhang, Z.; Fang, Y. One-Pot Synthesis of Two-Linker Mixed Al-Based Metal-Organic Frameworks for Modulated Water Vapor Adsorption. *Cryst. Growth Des.* **2020**, *20* (10), 6565–6572. https://doi.org/10.1021/acs.cgd.0c00747.

(10) Rieth, A. J.; Hunter, K. M.; Dincă, M.; Paesani, F. Hydrogen Bonding Structure of Confined Water Templated by a Metal-Organic Framework with Open Metal Sites. *Nat. Commun.* **2019**, *10* (1), 1–7. https://doi.org/10.1038/s41467-019-12751-z.

(11) Hunter, K. M.; Wagner, J. C.; Kalaj, M.; Cohen, S. M.; Xiong, W.; Paesani, F. Simulation Meets Experiment: Unraveling the Properties of Water in Metal-Organic Frameworks through Vibrational Spectroscopy. *J. Phys. Chem. C* **2021**, *125* (22), 12451–12460. https://doi.org/10.1021/acs.jpcc.1c03145.

(12) Brimmer, P. J.; Griffiths, P. R. ANGULAR DEPENDENCE OF

DIFFUSE REFLECTANCE INFRARED SPECTRA. PART III: LINEARITY OF KUBELKA-MUNK PLOTS. *Appl. Spectrosc.* **1988**, *42* (2), 242–247. https://doi.org/10.1366/0003702884428293.

(13) Brimmer, P. J.; Griffiths, P. R. Effect of Absorbing Matrixes on Diffuse Reflectance Infrared Spectra. *Anal. Chem.* **1986**, *58* (11), 2179–2184. https://doi.org/10.1021/ac00124a015.

(14) Sirita, J.; Phanichphant, S.; Meunier, F. C. Quantitative Analysis of Adsorbate Concentrations by Diffuse Reflectance FT-IR. *Anal. Chem.* **2007**, *79* (10), 3912–3918. https://doi.org/10.1021/ac0702802.

(15) Olinger, J. M.; Griffiths, P. R. Quantitative Effects of an Absorbing Matrix on Near-Infrared Diffuse Reflectance Spectra. *Anal. Chem.* **1988**, *60* (21), 2427–2435. https://doi.org/10.1021/ac00172a022.

(16) Salles, F.; Bourrelly, S.; Jobic, H.; Devic, T.; Guillerm, V.; Llewellyn, P.; Serre, C.; Ferey, G.; Maurin, G. Molecular Insight into the Adsorption and Diffusion of Water in the Versatile Hydrophilic/Hydrophobic Flexible MIL-53(Cr) MOF. *J. Phys. Chem. C* **2011**, *115* (21), 10764–10776. https://doi.org/10.1021/jp202147m.

(17) Dietzel, P. D. C.; Johnsen, R. E.; Blom, R.; Fjellvåg, H. Structural Changes and Coordinatively Unsaturated Metal Atoms on Dehydration of Honeycomb Analogous Microporous Metal-Organic Frameworks. *Chem. - A Eur. J.* **2008**, *14* (8), 2389–2397. https://doi.org/10.1002/chem.200701370.

(18) Furukawa, H.; Gándara, F.; Zhang, Y. B.; Jiang, J.; Queen, W. L.; Hudson, M. R.; Yaghi, O. M. Water Adsorption in Porous Metal-Organic Frameworks and Related Materials. *J. Am. Chem. Soc.* **2014**, *136* (11), 4369–4381. https://doi.org/10.1021/ja500330a.

(19) Hanikel, N.; Pei, X.; Chheda, S.; Lyu, H.; Jeong, W.; Sauer, J.; Gagliardi, L.; Yaghi, O. M. Evolution of Water Structures in Metal-Organic Frameworks for Improved Atmospheric Water Harvesting. *Science (80-.).* **2021**, *374* (6566), 454–459. https://doi.org/10.1126/science.abj0890.

(20) Zhang, H.; Snurr, R. Q. Computational Study of Water Adsorption in the Hydrophobic Metal-Organic Framework ZIF-8: Adsorption Mechanism and Acceleration of the Simulations. *J. Phys. Chem. C* **2017**, *121* (43), 24000–24010. https://doi.org/10.1021/acs.jpcc.7b06405.

(21) Calero, S.; Gómez-Álvarez, P. Underlying Adsorption Mechanisms of Water in Hydrophobic and Hydrophilic Zeolite Imidazolate Frameworks: ZIF-71 and ZIF-90. *J. Phys. Chem. C* **2015**, *119* (41), 23774–23780. https://doi.org/10.1021/acs.jpcc.5b07360.

(22) Mileo, P. G. M.; Ho Cho, K.; Park, J.; Devautour-Vinot, S.; Chang, J. S.; Maurin, G. Unraveling the Water Adsorption Mechanism in the Mesoporous MIL-100(Fe) Metal-Organic Framework. *J. Phys. Chem. C* **2019**, *123* (37), 23014–23025. https://doi.org/10.1021/acs.jpcc.9b06228.

(23) Babin, V.; Leforestier, C.; Paesani, F. Development of a "First Principles" Water Potential with Flexible Monomers: Dimer Potential Energy Surface, VRT Spectrum, and Second Virial Coefficient. *J. Chem. Theory Comput.* **2013**, *9* (12), 5395–5403. https://doi.org/10.1021/ct400863t.

(24) Babin, V.; Medders, G. R.; Paesani, F. Development of a "First Principles" Water Potential with Flexible Monomers. II: Trimer Potential Energy Surface, Third Virial Coefficient, and Small Clusters. *J. Chem. Theory Comput.* **2014**, *10* (4), 1599–1607. https://doi.org/10.1021/ct500079y.

(25) Medders, G. R.; Babin, V.; Paesani, F. Development of a "First-Principles" Water Potential with Flexible Monomers. III. Liquid Phase Properties. *J. Chem. Theory Comput.* **2014**, *10* (8), 2906–2910. https://doi.org/10.1021/ct5004115.

(26) Yin, W. H.; Xiong, Y. Y.; Wu, H. Q.; Tao, Y.; Yang, L. X.; Li, J. Q.; Tong, X. L.; Luo, F. Functionalizing a Metal-Organic Framework by a Photoassisted Multicomponent Postsynthetic Modification Approach Showing Highly Effective Hg(II) Removal. *Inorg. Chem.* **2018**, *57* (15), 8722–8725. https://doi.org/10.1021/acs.inorgchem.8b01457.

(27) Zhang, F. M.; Dong, H.; Zhang, X.; Sun, X. J.; Liu, M.; Yang, D. D.; Liu, X.; Wei, J. Z. Postsynthetic Modification of ZIF-90 for Potential Targeted Codelivery of Two Anticancer Drugs. *ACS Appl. Mater. Interfaces* **2017**, *9* (32), 27332–27337. https://doi.org/10.1021/acsami.7b08451.

(28) Dramstad, T. A.; Wu, Z.; Gretz, G. M.; Massari, A. M. Thin Films and Bulk Phases Conucleate at the Interfaces of Pentacene Thin Films. *J. Phys. Chem. C* **2021**, *125* (30), 16803–16809. https://doi.org/10.1021/acs.jpcc.1c04432.

(29) Neri, G.; Walsh, J. J.; Teobaldi, G.; Donaldson, P. M.; Cowan, A. J. Detection of Catalytic Intermediates at an Electrode Surface during Carbon Dioxide Reduction by an Earth-Abundant Catalyst. *Nat. Catal.* **2018**, *1* (12), 952–959. https://doi.org/10.1038/s41929-018-0169-3.

(30) Lu, H.; Huang, Y. C.; Hunger, J.; Gebauer, D.; Cölfen, H.; Bonn, M. Role of Water in CaCO3Biomineralization. *J. Am. Chem. Soc.* **2021**, *143* (4), 1758–1762. https://doi.org/10.1021/jacs.0c11976.

(31) Zhang, J.; Tan, J.; Pei, R.; Ye, S.; Luo, Y. Ordered Water Layer on the Macroscopically Hydrophobic Fluorinated Polymer Surface and Its Ultrafast Vibrational Dynamics. *J. Am. Chem. Soc.* **2021**. https://doi.org/10.1021/jacs.1c03581.

(32) Piontek, S. M.; Dellostritto, M.; Mandal, B.; Marshall, T.; Klein, M. L.; Borguet, E. Probing Heterogeneous Charge Distributions at the α-Al2O3(0001)/H2O Interface. *J. Am. Chem. Soc.* **2020**, *142* (28), 12096–12105. https://doi.org/10.1021/jacs.0c01366.

(33) Sudera, P.; Cyran, J. D.; Deiseroth, M.; Backus, E. H. G.; Bonn, M. Interfacial Vibrational Dynamics of Ice Ihand Liquid Water. *J. Am. Chem. Soc.* **2020**, *142* (28), 12005–12009. https://doi.org/10.1021/jacs.0c04526.

(34) Wang, C.; Zhang, T.; Lin, W. Rational Synthesis of Noncentrosymmetric Metal-Organic Frameworks for Second-Order Nonlinear Optics. *Chemical Reviews*. 2012, pp 1084–1104. https://doi.org/10.1021/cr200252n.

(35) McDermott, M. L.; Vanselous, H.; Corcelli, S. A.; Petersen, P. B. DNA's Chiral Spine of Hydration. *ACS Cent. Sci.* **2017**, *3* (7), 708–714. https://doi.org/10.1021/acscentsci.7b00100.

(36) Pullanchery, S.; Roke, S. Handy Water: Chiral Superstructures around Peptide β-Sheets. *Proc. Natl. Acad. Sci. U. S. A.* **2021**, *118* (2), 10–12. https://doi.org/10.1073/PNAS.2024376118.

(37) Wang, H.; Chen, W.; Wagner, J. C.; Xiong, W. Local Ordering of Lattice Self-Assembled SDS@2β-CD Materials and Adsorbed Water Revealed by Vibrational Sum Frequency Generation Microscope. *J. Phys. Chem. B* **2019**, *123* (29), 6212–6221. https://doi.org/10.1021/acs.jpcb.9b04928.

(38) Wang, H.; Wagner, J. C.; Chen, W.; Wang, C.; Xiong, W. Spatially Dependent H-Bond Dynamics at Interfaces of Water/Biomimetic Self-Assembled Lattice Materials. *Proc. Natl. Acad. Sci. U. S. A.* **2020**, *117* (38), 23385–23392. https://doi.org/10.1073/pnas.2001861117.

(39) Wang, H.; Xiong, W. Vibrational Sum-Frequency Generation Hyperspectral Microscopy for Molecular Self-Assembled Systems. *Annu. Rev. Phys. Chem.* **2020**, *72*, 279–306. https://doi.org/10.1146/annurev-physchem-090519-050510.

(40) Doughty, B.; Rao, Y.; Kazer, S. W.; Kwok, S. J. J.; Turro, N. J.; Eisenthal, K. B. Probing the Relative Orientation of Molecules Bound to DNA through Controlled Interference Using Second-Harmonic Generation. *Proc. Natl. Acad. Sci.* **2013**, *110* (15), 5756–5758. https://doi.org/10.1073/PNAS.1302554110.

(41) Rodriguez, D.; Marquez, M. D.; Zenasni, O.; Han, L. T.; Baldelli, S.; Lee, T. R. Surface Dipoles Induce Uniform Orientation in Contacting Polar Liquids. *Chem. Mater.* **2020**, *32* (18), 7832–7841. https://doi.org/10.1021/acs.chemmater.0c02471.

(42) Shen, Y. R. Surface Properties Probed by Second-Harmonic and Sum-Frequency Generation. *Nature* **1989**, *337* (6207), 519–525. https://doi.org/10.1038/337519a0.

(43) Wang, H.; Gao, T.; Xiong, W. Self-Phase-Stabilized Heterodyne Vibrational Sum Frequency Generation Microscopy. *ACS Photonics* **2017**, *4* (7), 1839–1845. https://doi.org/10.1021/acsphotonics.7b00411.

(44) Wang, H.; Gao, T.; Xiong, W. Self-Phase-Stabilized Heterodyne Vibrational Sum Frequency Generation Microscopy. *ACS Photonics* **2017**, *4* (7), 1839–1845. https://doi.org/10.1021/acsphotonics.7b00411.

(45) Miyamae, T.; Akiyama, H.; Yoshida, M.; Tamaoki, N. Characterization of Poly(N-Isopropylacrylamide)-Grafted Interfaces with Sum-Frequency Generation Spectroscopy. *Macromolecules* **2007**, *40* (13), 4601–4606. https://doi.org/10.1021/ma070399c.

(46) Xu, X.; Shen, Y. R.; Tian, C. Phase-Sensitive Sum Frequency

Vibrational Spectroscopic Study of Air/Water Interfaces: H 2 O, D 2 O, and Diluted Isotopic Mixtures. *J. Chem. Phys.* **2019**, *150* (14). https://doi.org/10.1063/1.5081135.

(47) Olenick, L. L.; Troiano, J. M.; Smolentsev, N.; Ohno, P. E.; Roke, S.; Geiger, F. M. Polycation Interactions with Zwitterionic Phospholipid Monolayers on Oil Nanodroplet Suspensions in Water (D2O) Probed by Sum Frequency Scattering. *J. Phys. Chem. B* **2018**, *122* (19), 5049–5056. https://doi.org/10.1021/acs.jpcb.8b00309.

(48) Lu, G.; Hupp, J. T. Metal-Organic Frameworks as Sensors: A ZIF-8 Based Fabry-Pérot Device as a Selective Sensor for Chemical Vapors and Gases. *J. Am. Chem. Soc.* **2010**, *132* (23), 7832–7833. https://doi.org/10.1021/ja101415b.

(49) Zheng, D. S.; Wang, Y.; Liu, A. A.; Wang, H. F. *Microscopic Molecular Optics Theory of Surface Second Harmonic Generation and Sum-Frequency Generation Spectroscopy Based on the Discrete Dipole Lattice Model*; 2008; Vol. 27. https://doi.org/10.1080/01442350802343981.

(50) Perets, E. A.; Yan, E. C. Y. Chiral Water Superstructures around Antiparallel β-Sheets Observed by Chiral Vibrational Sum Frequency Generation Spectroscopy. *J. Phys. Chem. Lett.* **2019**, *10* (12), 3395–3401. https://doi.org/10.1021/acs.jpclett.9b00878.

(51) G. Nicolau, B.; García-Rey, N.; Dryzhakov, B.; D. Dlott, D. Interfacial Processes of a Model Lithium Ion Battery Anode Observed, in Situ, with Vibrational Sum-Frequency Generation Spectroscopy. *J. Phys. Chem. C* **2015**, *119* (19), 10227–10233. https://doi.org/10.1021/acs.jpcc.5b01290.

(52) Lin, S. T.; Maiti, P. K.; Goddard, W. A. Two-Phase Thermodynamic Model for Efficient and Accurate Absolute Entropy of Water from Molecular Dynamics Simulations. *J. Phys. Chem. B* **2010**, *114* (24), 8191–8198. https://doi.org/10.1021/jp103120q.

(53) Phys, J. C.; Lin, S.; Blanco, M.; Goddard, W. A. The Two-Phase Model for Calculating Thermodynamic Properties of Liquids from Molecular Dynamics : Validation for the Phase Diagram of Lennard-Jones Fluids. **2017**, *11792* (2003). https://doi.org/10.1063/1.1624057.

(54) Pascal, T. A.; Lin, S. T.; Goddard, W. A. Thermodynamics of Liquids: Standard Molar Entropies and Heat Capacities of Common Solvents from 2PT Molecular Dynamics. *Phys. Chem. Chem. Phys.* **2011**, *13* (1), 169–181. https://doi.org/10.1039/c0cp01549k.

(55) Shrestha, B. R.; Pillai, S.; Santana, A.; Donaldson, S. H.; Pascal, T. A.; Mishra, H. Nuclear Quantum Effects in Hydrophobic Nanoconfinement. *J. Phys. Chem. Lett.* **2019**, *10* (18), 5530–5535. https://doi.org/10.1021/acs.jpclett.9b01835.

(56) Wang, D.; Yang, D.; Huang, C.; Huang, Y.; Yang, D.; Zhang, H.; Liu, Q.; Tang, T.; Gamal El-Din, M.; Kemppi, T.; Perdicakis, B.; Zeng, H. Stabilization Mechanism and Chemical Demulsification of Water-in-Oil and Oil-in-Water Emulsions in Petroleum Industry: A Review. *Fuel* **2021**, *286* (P1), 119390. https://doi.org/10.1016/j.fuel.2020.119390.

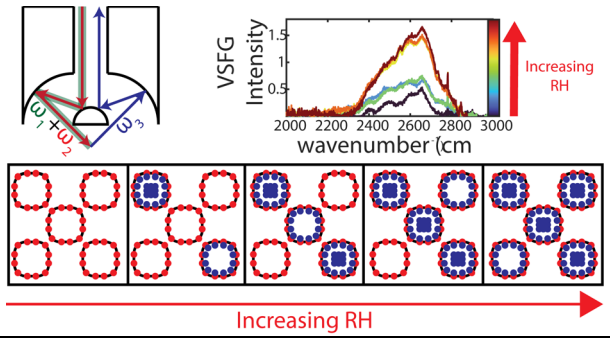

For Table of Contents Only